Mast cells in advanced atherosclerosis: from human plaque stability to new therapeutic targets

Hemme, E.

Chapter 4

Bruton's Tyrosine Kinase inhibition by Acalabrutinib does not affect early or advanced atherosclerotic plaque size and morphology in *Ldlr*$^{-/-}$ mice

Esmeralda Hemme[1], Danique Biskop[1], Marie A.C. Depuydt[1], Virginia Smit[1], Lucie Delfos[1], Mireia N.A. Bernabé Kleijn[1], Amanda C. Foks[1], Johan Kuiper[1], Ilze Bot[1]

Vascular Pharmacology. 2023 Jun 6; 150:107172

[1]Division of BioTherapeutics, Leiden Academic Centre for Drug Research, Leiden University, Leiden, The Netherlands

Abstract

Background: Atherosclerosis is characterized by the accumulation of lipids and immune cells, including mast cells and B cells, in the arterial wall. Mast cells contribute to atherosclerotic plaque growth and destabilization upon active degranulation. The FcεRI-IgE pathway is the most prominent mast cell activation route. Bruton's Tyrosine Kinase (BTK) is involved in FcεRI-signaling and may be a potential therapeutic target to limit mast cell activation in atherosclerosis. Additionally, BTK is crucial in B cell development and B-cell receptor signaling. In this project, we aimed to assess the effects of BTK inhibition on mast cell activation and B cell development in atherosclerosis.

Methods and Results: In human carotid artery plaques, we showed that BTK is primarily expressed on mast cells, B cells and myeloid cells. *In vitro*, BTK inhibitor Acalabrutinib dose-dependently inhibited IgE mediated activation of mouse bone marrow derived mast cells. *In vivo*, male *Ldlr*$^{-/-}$ mice were fed a high-fat diet for eight weeks, during which mice were treated with Acalabrutinib or control solvent. In Acalabrutinib treated mice, B cell maturation was reduced compared to control mice, showing a shift from follicular II towards follicular I B cells. Mast cell numbers and activation status were not affected. Acalabrutinib treatment did not affect atherosclerotic plaque size or morphology. In advanced atherosclerosis, where mice were first fed a high-fat diet for eight weeks before receiving treatment, similar effects were observed.

Conclusion: Conclusively, BTK inhibition by Acalabrutinib alone did neither affect either mast cell activation nor early- and advanced atherosclerosis, despite the effects on follicular B cell maturation.

Introduction

Cardiovascular diseases (CVD), including myocardial infarction and stroke, are responsible for high mortality rates in the Western society. The main underlying pathology of many CVD is atherosclerosis, which is a chronic autoimmune-like disease characterized by the accumulation of lipids and immune cells in the arterial wall. Over time, atherosclerotic plaques progress and can become unstable by thinning of the fibrous cap. Unstable plaques are prone to plaque rupture, which can lead to thrombus formation and occlusion of arteries leading to clinical manifestations such as myocardial infarction or stroke. Currently, patients with CVD are generally treated with lipid-lowering therapy, such as statins[1]. However, the high mortality rates suggest that current therapies remain largely inadequate to halt the progression of atherosclerosis and prevent CVD. Therefore, there is an urgent need to discover new pharmacological treatments to prevent atherosclerotic plaque development and progression towards unstable plaques. A potential target cell could be the mast cells, since accumulating evidence established a crucial role for mast cells in atherosclerotic plaque progression and destabilization.[2]

Mast cells are tissue resident pro-inflammatory innate immune cells that are mainly involved in host defense mechanisms against pathogens and known for their contribution to diseases such as allergy and asthma[3]. Various studies have also revealed a crucial role for mast cells in atherosclerosis. Experimental models have shown that mast cells contribute to atherosclerotic plaque development and destabilization via the excretion of pro-inflammatory cytokines, chemokines and neutral proteases, such as tryptase and chymase[4,5]. In human atherosclerotic plaques, mast cells accumulate during plaque progression and associate with an unstable plaque phenotype and the incidence of intraplaque hemorrhage[6]. Moreover, clinically highly relevant is the observation that intraplaque mast cell numbers also associate with the occurrence of future cardiovascular events[6], emphasizing the potential impact of mast cells on plaque stability.

Mast cells exert their effects due to release of pro-inflammatory and proteolytic mediators upon active degranulation via dedicated mast cell activation pathways. In allergy, the most prominent mast cell activation pathway is via crosslinking of the Fcε-receptors (FcεR) with immunoglobulin E (IgE) – antigen complexes[7]. FcεR-mediated mast cell activation may also contribute to atherosclerotic plaque growth and destabilization. Wezel and colleagues, for example, highlighted the contribution of the FcεRI-mediated pathway in atherosclerosis, as IgE administration in *ApoE*$^{-/-}$*uMT*$^{-/-}$ mice, that lack endogenous IgE, resulted in increased mast cell activation and atherosclerotic plaque size[8]. Interestingly, also in human atherosclerotic plaques the IgE-FcεR-mediated pathway is suggested to be a major mast cell activation pathway, since most activated plaque-derived mast cells were found to have IgE bound on their cell surface[9].

Previously, anti-IgE neutralizing antibodies were used as a strategy to intervene with the IgE-FcεR-mediated pathway in a mouse model for atherosclerosis, which resulted in less perivascular mast cell activation and successfully inhibited atherosclerosis progression[10]. Alternatively, Bruton's Tyrosine Kinase (BTK) can be used as a therapeutic target to limit mast cell activation in atherosclerosis. BTK is a cytoplasmic nonreceptor tyrosine kinase that is involved in FcεR-dependent mast cell activation and degranulation. After binding of IgE-antigen complexes to the Fcε-receptor, downstream proteins Lyn and Syk become phosphorylated, which in turn results in phosphorylation of BTK. Fully phosphorylated BTK leads to phosphorylation of PLCγ2 and eventually leads to mast cell degranulation and production of inflammatory cytokines[11]. Previously, research showed that BTK inhibition using an FDA approved selective BTK inhibitor, called Acalabrutinib, prevents IgE-mediated degranulation and cytokine release in primary human skin-derived mast cells (SDMCs)[12].

An additional advantage of targeting BTK in atherosclerosis is its crucial role in B cell development and B-cell receptor (BCR) signaling. B cells contribute to atherosclerosis progression by antibody secretion, cytokine secretion and T cell regulation[13]. B cell activation, proliferation, and differentiation is mainly controlled by BCR signaling. Similar as in mast cells, BCR stimulation induces BTK phosphorylation via Lyn and Syk. Therapeutic modulation of BCR signaling may affect B cell subset distribution, which in turn could affect atherogenesis.

Currently, several FDA-approved BTK inhibitors are used to treat various B cell driven malignancies, such as chronic lymphocytic leukemia (CLL)[14,15]. In these patients, BTK inhibition therapy is well tolerated and shows durable remissions, which is beneficial for disease outcome. In recent years, targeting BTK has become of increasing interest in autoimmune diseases as well, since B cells are also involved in the pathogenesis of, for example, rheumatoid arthritis (RA) and multiple sclerosis (MS). Preclinical experiments in animal models of collagen-induced arthritis (CIA) and clinical trials in MS patients provided evidence showing that BTK inhibition effectively reduces autoimmune symptoms, such as immune cell infiltration and autoantibody production[16,17]. Atherosclerosis is being considered an autoimmune-like disease[18] with, amongst others, an important mast cell component in disease progression[2]. BTK is essentially involved in the FcεR signaling pathway, which is a prominent activation route of mast cells, also in advanced atherosclerosis, thereby contributing to atherosclerotic plaque destabilization.

In this project, we thus aimed to assess BTK expression in human carotid artery plaques and the effects of BTK inhibition on both mast cell activation and B cell development in a mouse model of atherosclerosis. We hypothesized that BTK inhibition reduces both mast cell activation and B cell maturation, leading to protection against atherosclerosis progression.

Materials and Methods

Single-cell RNA sequencing

Human carotid artery plaques were collected from 18 patients (14 male, 4 female) that underwent carotid endarterectomy surgery as part of AtheroExpress, an ongoing biobank study at the University Medical Centre Utrecht[19]. Single cells were obtained and processed for single-cell RNA sequencing as previously described[20]. Data were processed and clustered as previously described[20]. All studies were performed in accordance with the Declaration of Helsinki. Informed consent was obtained from all subjects involved in the study.

Atherosclerotic aortic arches, from which perivascular adipose tissue was removed, were isolated from female *Ldlr*$^{-/-}$ mice and enzymatically digested. Single cell suspensions were stained with Fixable Viability Dye eFluor™ 780 (1:2000, eBioscience) and CD45-PE (1:500, clone 30-F11, Biolegend). After removing doublets, alive CD45^{+} cells were sorted using a FACS Aria II SORP (BD Biosciences) and loaded on a Chromium Single Cell instrument (10x Genomics) to prepare single-cell RNA-sequencing (scRNA seq) libraries. Sequencing was performed on an Illumina HiSeq2500 and the digital expression matrix was generated by de-multiplexing barcode processing and gene UMI (unique molecular index) counting using the Cell Ranger pipeline (10x Genomics).

Digital expression matrices were analyzed using the Seurat package in R. Low quality cells were excluded by setting thresholds for unique gene count reads and mitochondrial gene expression. Using the DoubletDecon approach, doublets were removed and remaining transcriptomes were clustered into 16 clusters. *Cd19*$^{+}$ B cell clusters were selected and filtered by setting thresholds for *Cd3e*<0.3 and *Cd68*<0.3 to exclude non-B-cells. *Cd68*$^{+}$ and *Itgam*$^{+}$ myeloid clusters were selected and filtered by setting thresholds for *Cd3e*<0.3, *Cd19*<0.3, *Cd79b*<0.3 to exclude non-myeloid cells. Mast cells were selected and filtered by setting thresholds for *Kit*>0.3, *Cpa3*>0.3.

Cell culture

Bone marrow derived mast cells (BMMCs) derived from C57BL/6 mice were cultured in RPMI 1640 containing 25 mM HEPES (VWR) and supplemented with 10% fetal bovine serum (Sigma-Aldrich, The Netherlands), 1% L-Glutamine (biowest, France), 100 U/mL mix of penicillin/streptomycin (Gibco, USA), 1% sodium pyruvate (Sigma-Aldrich), 1% non-essential amino acids (MEM NEAA; Gibco) and 5 ng/mL IL-3 (Immunotools). Cells were incubated at 37^{o}C and 5% CO_2 and were kept at a density of $0.25*10^6$ cells/mL by weekly subculturing. BMMCs were cultured for four weeks in total to obtain mature mast cells. Mast cell purity was assessed by measuring CD117 and FcεRIα expression using flow cytometry and purity was routinely found to be above 98%.

Mast cell activation assay

Acalabrutinib stock was dissolved in DMSO and stored in -80°C. Fresh dilutions from Acalabrutinib stock were prepared in sterile PBS prior to each experiment. Mature BMMCs were plated at 1 × 10^6/mL and treated with varying concentrations of Acalabrutinib ranging from 1 nm to 100 µM at 37°C for 1 hour. As Acalabrutinib was dissolved in DMSO, vehicle control BMMCs were pretreated with DMSO with an equivalent volume to the highest Acalabrutinib concentration. BMMCs were sensitized with antiDNP-IgE (1 µg/mL, Sigma-Aldrich) for 2.5 hours and activated with DNP-HSA (20 ng/mL, Sigma-Aldrich) for 30 minutes. Negative control remained unstimulated. Mast cell activation was measured with flow cytometry as percentage $CD63^+$ of $CD117^+$ $Fc\varepsilon RI\alpha^+$ mast cells.

Animal experiments

All animal work was performed in compliance with the guidelines of the Dutch government and the Directive 2010/63/EU of the European Parliament. The experiment was approved by the Ethics Committee for Animal Experiments and the Animal Welfare Body of Leiden University (Project 106002017887, Study number 887,1-67). Low-density lipoprotein receptor-deficient mice (*Ldlr*$^{-/-}$) on a C57BL/6 background were bred in-house. All animals were kept under standard laboratory conditions and diet and water were provided ad libitum. Two separate *in vivo* studies were performed, a prevention and therapeutic study. In both studies, mice were randomized in groups based on age, weight and serum total cholesterol levels. For the prevention study, 9 to 14 weeks old male *Ldlr*$^{-/-}$ mice were fed a high-fat diet (HFD) containing 0.25% cholesterol and 15% cocoa butter (Special Diet Services, cat. Nr. 824171, Witham, Essex, U.K.) for eight weeks to induce atherosclerotic plaque formation. Mice received either BTK inhibitor Acalabrutinib (25 mg/kg; n=15; MedChemExpress, USA) or control solvent (2% DMSO, 30% PEG300, 2% Tween-80 in phosphate buffered saline (PBS); n=15) three times per week by oral gavage. For the therapeutic study, male *Ldlr*$^{-/-}$ mice were first placed on a HFD for eight weeks before starting eight weeks of treatment with Acalabrutinib or control solvent (three times per week by oral gavage). At the start of the treatment, mice were 12 to 17 weeks old and one group was sacrificed as a baseline group. During treatment, mice were weighed weekly and blood was collected by tail vein bleeding. A detailed overview of the prevention and therapeutic study is provided in Supplement Figure 2 and 4, respectively. At sacrifice, all mice were euthanized using subcutaneous administration of anaesthetics (ketamine (40 mg/mL), atropine (0.1 mg/mL) and xylazine (8 mg/mL)). Blood was collected via orbital bleeding, after which the mice were perfused with PBS through the left cardiac ventricle. Next, organs were collected for further analysis.

Cholesterol assay

Serum was collected through centrifugation at 8000 rpm for 10 minutes at 4°C and stored at -80°C until further use. Total cholesterol levels in serum were determined using an enzymatic

colorimetric procedure (Roche/Hitachi, Germany). Precipath standardized serum (1.69 mg/mL, Roche/Hitachi) was used as an internal standard.

Cell suspensions

At sacrifice, aortic arch, blood, spleen, mediastinal lymph nodes (mLN) and peritoneal cells were isolated. Single cell suspensions of spleen and mLN were obtained by mashing the organs through a 70 µm cell strainer. Red blood cells were removed from blood and splenocytes by lysing samples for two minutes with ACK lysis buffer (0.15 M NH4Cl, 10 mM NaHCO3, 0.1 mM EDTA, pH 7.3). Aortic arches were digested with 450 U/mL collagenase I, 250 U/mL collagenase XI, 120 U/mL DNAse, and 120 U/mL hyaluronidase for 30 minutes at 37°C, and subsequently strained through 70 µm cell strainers Single cell suspensions were analyzed by flow cytometry.

Flow cytometry

Single cell suspensions were extracellularly stained with anti-mouse fluorochrome-conjugated antibodies for 30 minutes at 4^{o}C. Fc block was used to block Fc receptors to prevent aspecific binding of antibodies. Live/dead viability staining was used for exclusion of non-viable cells. Prior to intracellular staining, cells were fixed and permeabilized according to manufacturer's protocol (Invitrogen, transcription factor: Transcription factor FoxP3 Buffer Set). After fixation and permeabilization, cells were intracellularly stained for 30 minutes at 4^{o}C. All antibodies used for flow cytometry are listed in Table S1. Flow cytometry measurements were performed on a CytoFLEX S (Beckman Coulter, USA). Data were analyzed using FlowJo v10.7 software (Treestar). Flow cytometry markers used for leukocyte identification are specified in Table S2.

Legendplex assay

Immunoglobulin concentrations were measured in serum using LEGENDplex™ Immunoglobulin Isotyping Panel assay (Biolegend) according to manufacturer's instructions. LEGENDplex™ measurements were performed on a CytoFLEX S (Beckman Coulter, USA).

Serum IgE measurement

Serum was collected through centrifugation at 8000 rpm for 10 minutes at 4°C and stored at -80°C until further use. IgE was measured using an IgE ELISA kit (Biolegend) according to manufacturer's instructions.

Histological analysis

Hearts were isolated, embedded and frozen in Tissue-Tek OCT compound (Sakura). Per slide, ten 5 µm-thick cryosections of the aortic root were collected with 50 µm distance between each section using a Leica CM1950 cryostat. Atherosclerotic plaque size and the percentage stenosis was determined by Oil-Red-O (ORO) staining in five subsequent sections of the aortic root to cover the entire area from the start to the end of the aortic valves. Masson's trichrome staining (Sigma-Aldrich) was performed to assess plaque collagen content in three subsequent

sections of the three-valve area containing the largest plaques. Corresponding sections were stained immunohistochemically with an antibody directed against a macrophage-specific antigen (MOMA-2, monoclonal rat IgG2b, diluted 1:1000). Biotinylated rabbit anti-rat IgG (BA-4001, Vector, dilution 1:200) was used as a secondary antibody and the reaction was visualized with ImPACT NovaRED Peroxidase (HRP) substrate (Vector). Sections were digitalized using a Panoramic 250 Flash III slide scanner (3DHISTECH, Hungary). Analysis was performed using ImageJ software. A Naphthol AS-D chloroacetate staining (Sigma-Aldrich) was performed to manually quantify resting and activated adventitial mast cells in three subsequent sections of the aortic root. Mast cells were identified and counted in the perivascular tissue of the aortic root at the site of atherosclerosis. Absolute mast cell counts were normalized to tissue area to determine the total number of mast cells per mm^2 perivascular tissue. A mast cell was considered resting when all granules were maintained inside the cell, while mast cells were assessed as activated when granules were deposited in the tissue surrounding the mast cell.

Statistical analysis

Data analysis was performed using Prism 9.0 (GraphPad Software, Inc. San Diego, CA, USA). Data are expressed as mean ± SEM for all analyses. Outliers were identified by a Grubbs' test. Shapiro-Wilkson normality test was used to test data for normal distribution. An unpaired two-tailed Student t-test or an ordinary one-way ANOVA test with Tukey multiple comparison test was used to compare normally distributed data between two or more than two groups, respectively. A Mann-Whitney U test or Kruskal-Wallis test with Dunn's multiple comparisons test was performed for not normally distributed data between two or more than two groups, respectively. Probability values of $P < 0.05$ were considered significant.

Results

Bruton's Tyrosine Kinase is expressed on mast cells, B cells and myeloid cells in human carotid artery plaques and in mouse atherosclerotic aortas

First, we aimed to determine the expression levels of *BTK* in human atherosclerotic plaque cell subsets. Previously, the cellular transcriptome of human carotid artery plaques of 18 patients (77% male) obtained from carotid endarterectomy surgery was established using single-cell RNA sequencing (scRNA seq) technology[20]. In this study, fourteen distinct cell clusters were identified, among which three non-immune cell clusters and eleven leukocyte clusters including T cells, B cells, mast cells and myeloid cells (Figure 1A). In this dataset, we analyzed the distribution of *BTK* expression amongst cell clusters in these advanced atherosclerotic plaques. In line with literature[21,22], *BTK* expression was found in B cells, myeloid cells and the most abundant expression was found in the mast cell cluster (Figure 1B). Signature genes confirmed the B cell (*CD19*), myeloid (*CD68*) and mast cell (*KIT*) cluster identities in human carotid artery plaques (Supplement Figure 1A). Additionally, we confirmed *Btk* expression in

mast cells, B cells and myeloid cells in the single-cell transcriptome of atherosclerotic aortas of *Ldlr*$^{-/-}$ mice (Supplement Figure 1B).

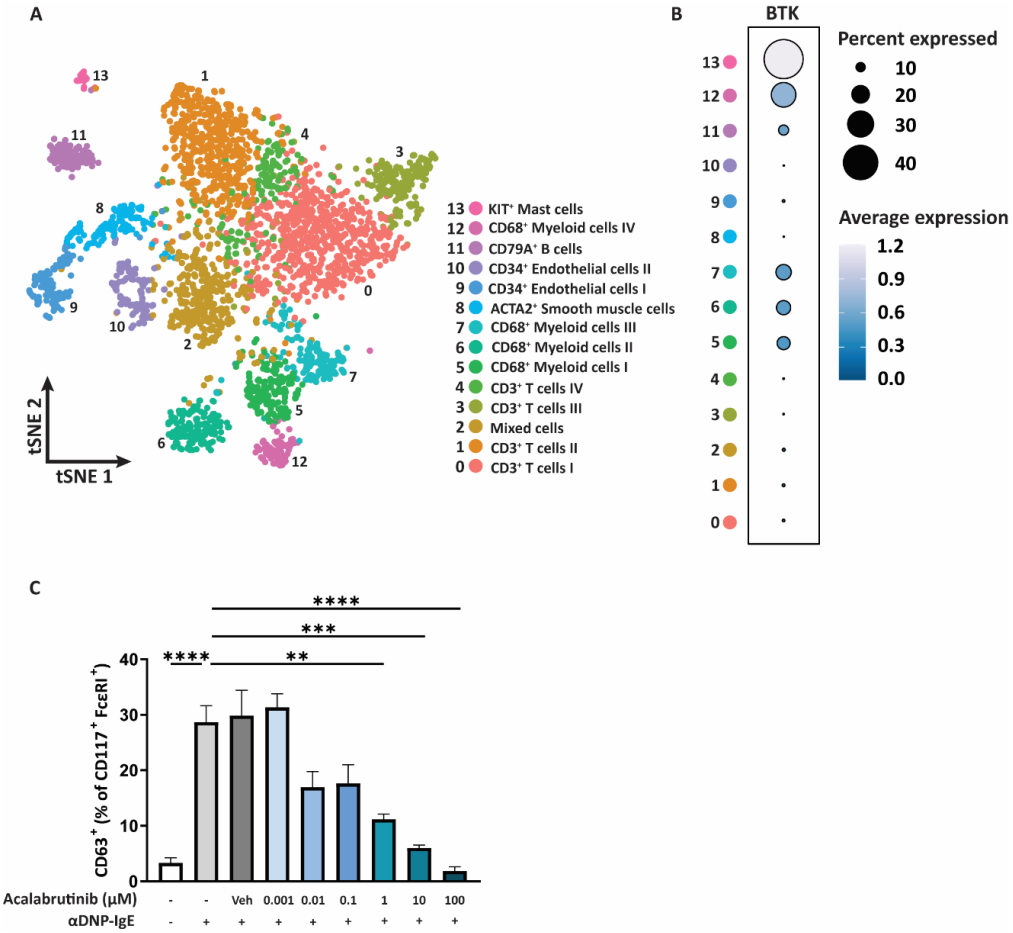

Figure 1. A) Single-cell RNA sequencing of human carotid artery plaques revealed 14 distinct cell clusters. B) DotPlot visualization of Bruton's Tyrosine Kinase (*BTK*) expression in human carotid artery plaque cell clusters, showing most expression in mast cells (13), B cells (11) and myeloid cell clusters (5-7, 12). C) Percentage CD63^{+} was measured in CD117^{+}FcεRI^{+} bone marrow derived mast cells (BMMCs) by flow cytometry. Acalabrutinib dose-dependently reduced IgE-induced mast cell activation. Veh is vehicle control. Data are shown as mean ± SEM of three independent experiments performed with BMMCs isolated from three different donor mice. ** $p < 0.01$, *** $p < 0.001$, **** $p < 0.0001$.

Acalabrutinib dose-dependently inhibits bone marrow-derived mast cell activation *in vitro*

Previous studies showed the ability of BTK inhibitors to inhibit IgE-mediated activation of human mast cells[12]. Here, we confirmed the efficacy of BTK inhibitor Acalabrutinib to inhibit mouse BMMC activation via the FcεR-mediated pathway *in vitro*. As shown in Figure 1C, treatment of BMMCs with increasing concentrations of Acalabrutinib reduced IgE-mediated mast cell activation as measured by CD63 expression[23] in a dose-dependent manner. A significant reduction of BMMC activation was achieved from treatment with 1 μM (11.2 ± 0.9 %; $p = 0.003$) and higher compared to the untreated activated BMMCs (positive control; 28.7 ± 1.0 %). Acalabrutinib did not affect BMMC viability, since all treatment conditions showed a

cell viability percentage above 98% (Supplement Figure 1C). Collectively, these data suggest that Acalabrutinib dose-dependently inhibits BMMC activation *in vitro*.

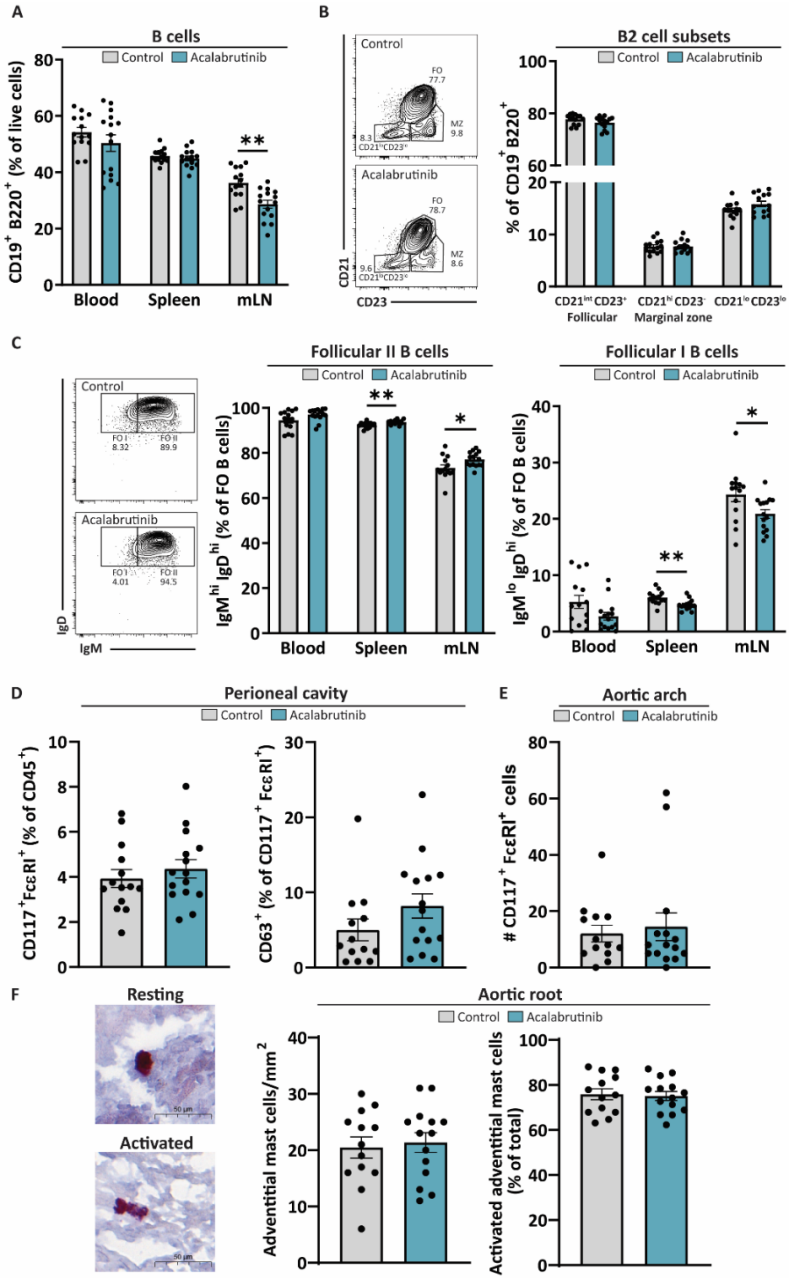

Figure 2. Acalabrutinib treatment decreased B cell maturation, but did not affect mast cell activation in initial atherosclerosis. A) Flow cytometry quantification of $CD19^+$ $B220^+$ B cells in blood, spleen and mLN. B) Representative flow charts and quantification of follicular ($CD21^{int}$ $CD23^+$), marginal zone ($CD21^{hi}$ $CD23^-$) and newly formed ($CD21^{lo}$ $CD23^{lo}$) B cells in the spleen. C) Representative flow charts and quantification of immature follicular II (FO II; IgM^{hi} IgD^{hi}) and mature follicular I (FO I; IgM^{lo} IgD^{hi}) B cells in blood, spleen and mLN showing a shift from FO I towards FO II B cells. D) Flow cytometry quantification of $CD117^+$ $Fc\varepsilon RI^+$ mast cells and $CD63^+$ mast cells in the peritoneal cavity. E) Flow cytometry quantification of $CD117^+$ $Fc\varepsilon RI^+$ mast cells in the aortic arch. F) Napthol AS-D chloroacetate staining of a resting (top) and activated (bottom) mast cell in the adventitia of the aortic root. Scale bar indicates 50 µM. Histological quantification of total (left) and percentage activated (right) adventitial mast cells in the aortic root. Data represent mean ± SEM. * $p < 0.05$, ** $p < 0.01$

BTK inhibition by Acalabrutinib reduced systemic B cell maturation

To assess the effect of BTK inhibition on early-stage atherosclerosis in a prevention study, male *Ldlr*$^{-/-}$ mice were treated with Acalabrutinib for eight weeks while being fed an HFD. A graphical overview of the atherosclerosis prevention study is shown in Supplement Figure 2. During the experiment, body weight and serum total cholesterol levels did not differ between the control and treatment group (Supplement Figure 2).

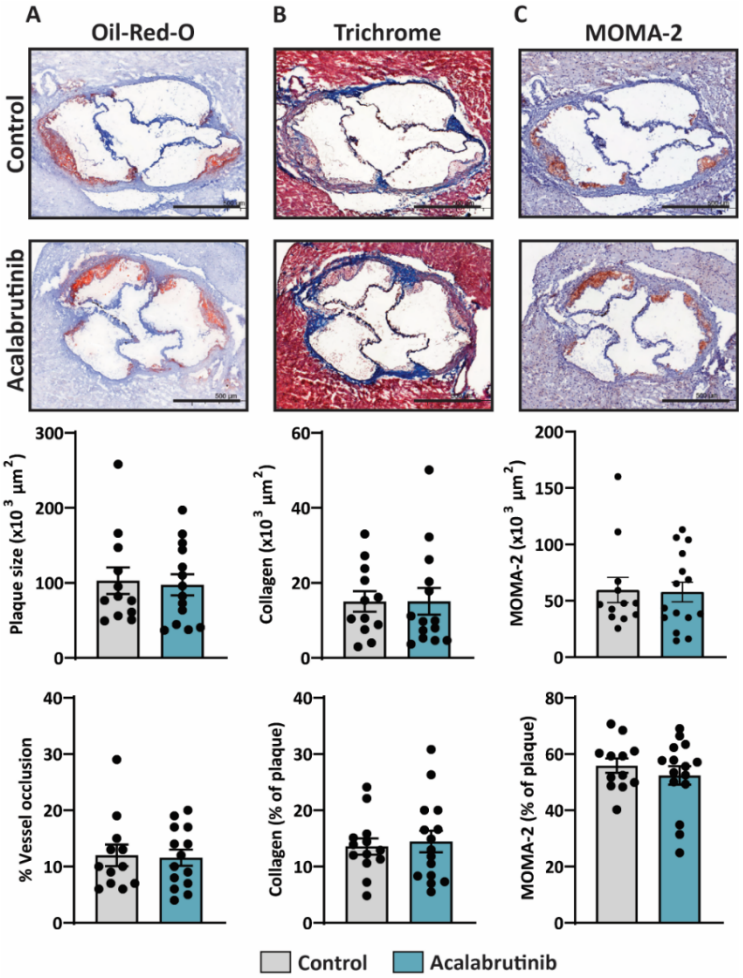

Figure 3. BTK inhibition did not affect plaque size and composition in a prevention *in vivo* set-up. A, vertical) Oil-Red-O staining, showing that Acalabrutinib treatment did not affect absolute plaque size and vessel occlusion (percentage plaque area of total vessel area). B, vertical) Masson's Trichrome staining to determine absolute and percentage collagen content of the plaque. C, vertical) monocyte/macrophage staining (clone MOMA-2) to determine absolute and percentage macrophage content of the plaque. All representative pictures are taken at optical magnification 5x. Scale bars indicate 500 µm. Data are shown as mean ± SEM.

Previously, the importance of BTK in BCR signaling and B cell development and differentiation has been described[24]. Therefore, blood, spleen and mLNs were isolated to examine the effects of BTK inhibition on B cells in early-stage atherosclerosis using flow cytometry. In line with literature, BTK inhibition in atherosclerosis did not affect circulating and splenic CD19^{+} B220^{+} B cell frequencies (Figure 2). The percentage of CD19^{+} B220^{+} B cells were significantly

decreased in mLNs of Acalabrutinib treated mice (Figure 2A). Analysis of the B2 cell lineage ($CD19^+$ $B220^+$ $CD93^-$), the main B cell lineage present in atherosclerosis[13], did not reveal any differences between follicular ($CD21^{int}$ $CD23^+$), marginal zone ($CD21^{hi}$ $CD23^-$) and newly formed ($CD21^{lo}$ $CD23^{lo}$) B cells in the spleen, circulation and mLN of both groups (Figure 2B and Supplement Figure 3A-B).

BTK inhibitors are however known to specifically affect B cell maturation and activation as demonstrated in a mouse model of multiple sclerosis[24]. Therefore, we assessed maturation of follicular B cells in blood, spleen and mLNs in our atherosclerosis model as well. Indeed, we observed a significant increase in splenic immature follicular II (FO II; IgM^{hi} IgD^{hi}) in Acalabrutinib treated mice (93.7 ± 0.3 %) compared to control mice (92.4 ± 0.3 %; p = 0.005), while mature follicular I (FO I; IgM^{lo} IgD^{hi}) B cells (Acalabrutinib: 4.7 ± 0.3 %; control: 6.0 ± 0.3 %; p = 0.004) were significantly decreased. A similar effect was observed for follicular B cells in mLNs. These data confirm that Acalabrutinib successfully inhibited BTK *in vivo* and that BTK inhibition leads to a shift towards less B cell maturation in atherosclerosis. Despite the effect on B cell maturation, circulating antibody levels remained unaffected (Supplement Figure 3C).

Acalabrutinib treatment did not affect mast cell activation and myeloid cells in early atherosclerosis

Next, we examined systemic mast cell activation in response to BTK inhibition in the peritoneal cavity. As shown in Figure 2D, Acalabrutinib treatment did not affect mast cell frequency and activation status, as measured by CD63 expression. Absolute mast cell numbers in the aortic arch did not differ between Acalabrutinib treated mice (14.5 ± 4.9) and control mice (12.1 ± 2.9; Figure 2E). In addition, no differences were observed in the total number of adventitial mast cells in the aortic root as measured by histology. BTK inhibition by Acalabrutinib in this initial stage of atherosclerosis also did not affect the percentage and absolute number of activated mast cells compared to control treated mice (75.1 ± 2.0 % versus 75.9 ± 2.4 %; Figure 2F and S3). These data suggest that BTK inhibition does not affect mast cell activation in early atherosclerosis.

Increasing evidence also suggest an essential role for BTK in myeloid cells, such as monocytes and macrophages[21,25]. Therefore, we examined circulating monocytes and myeloid cell frequencies in the spleen showing that Acalabrutinib treatment did not significantly affect myeloid cells systemically (Supplement Figure 4).

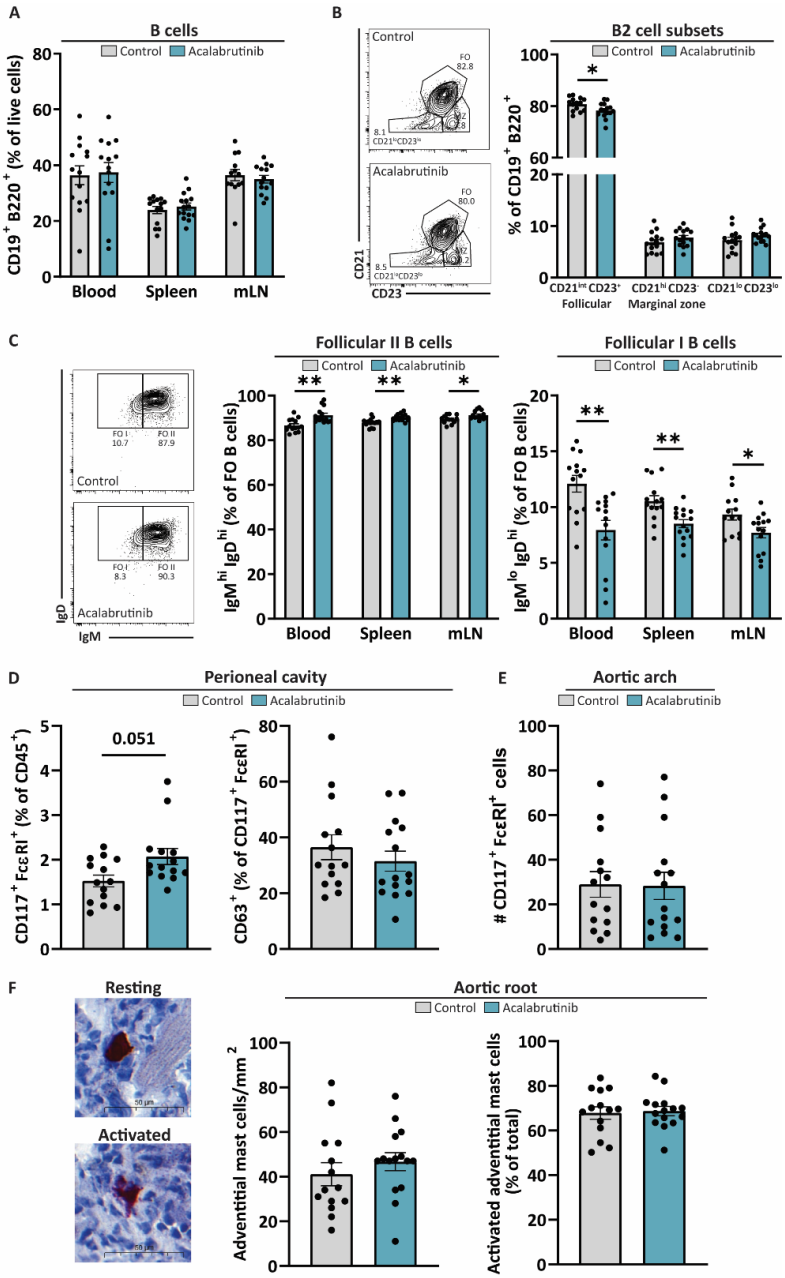

Figure 4. Acalabrutinib treatment decreased B cell maturation, but did not affect mast cell activation in a therapeutic *in vivo* set-up. A) Flow cytometry quantification of $CD19^+$ $B220^+$ B cells in blood, spleen and mLN. B) Representative flow charts and quantification of follicular ($CD21^{int}$ $CD23^+$), marginal zone ($CD21^{hi}$ $CD23^-$) and newly formed ($CD21^{lo}$ $CD23^{lo}$) B cells in the spleen. C) Representative flow charts and quantification of immature follicular II (FO II; IgM^{hi} IgD^{hi}) and mature follicular I (FO I; IgM^{lo} IgD^{hi}) B cells in blood, spleen and mLN showing a shift from FO I towards FO II B cells. D) Flow cytometry quantification of $CD117^+$ $Fc\varepsilon RI^+$ mast cells and $CD63^+$ mast cells in the peritoneal cavity E) Flow cytometry quantification of $CD117^+$ $Fc\varepsilon RI^+$ mast cells in the aortic arch. F) Napthol AS-D chloroacetate staining of a resting (top) and activated (bottom) mast cell in the adventitia of the aortic root. Scale bar indicates 50 µM. Histological quantification of total (left) and percentage activated (right) adventitial mast cells in the aortic root. Data represent mean ± SEM. * $p < 0.05$, ** $p < 0.01$

BTK inhibition did not affect plaque size and composition in a prevention study set-up

Furthermore, we examined whether BTK inhibition via Acalabrutinib affected atherosclerotic plaque size. BTK inhibition did not protect against plaque development, as absolute plaque size and the percentage of vascular stenosis did not differ between Acalabrutinib (97.5 ± 14.0 x 10^3 µm^2) and vehicle control treated mice (102.9 ± 17.7 x 10^3 µm^2; Figure 3A). In addition, collagen content was not affected by BTK inhibition compared to control mice (Figure 3B). Lastly, monocyte/macrophage content locally within the atherosclerotic plaques was determined by MOMA-2 staining. As shown in Figure 3C, both the absolute macrophage area and the percentage MOMA-2 staining were comparable between mice treated with Acalabrutinib and control mice.

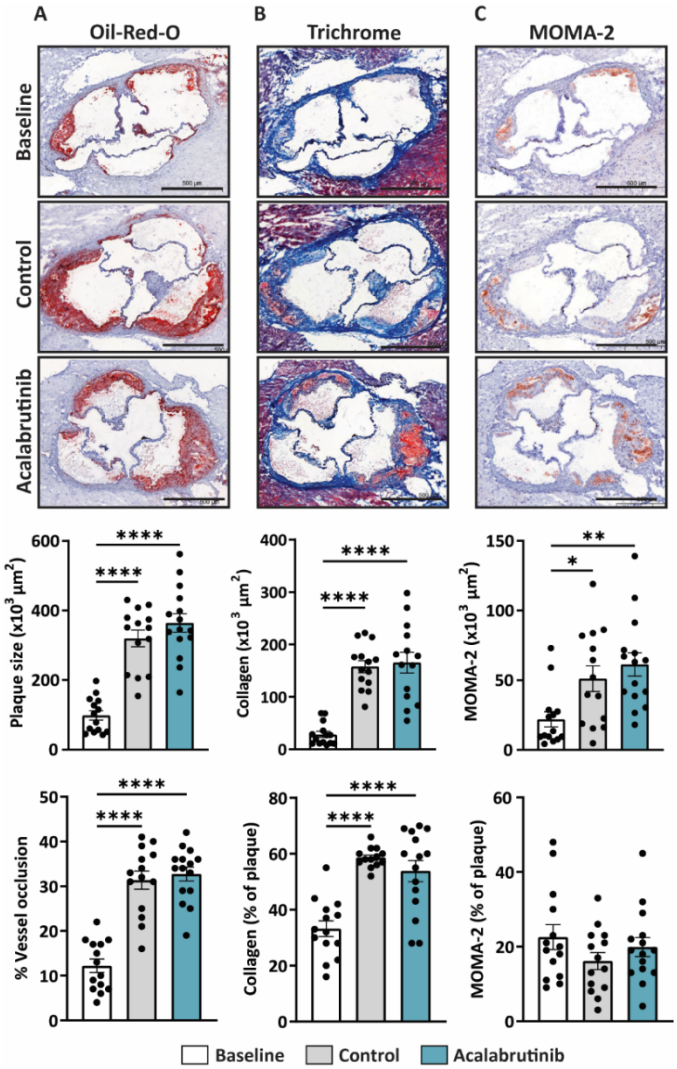

Figure 5. BTK inhibition did not affect plaque size and morphology in a therapeutic *in vivo* set-up. A, vertical) Oil-Red-O staining, showing that Acalabrutinib treatment did not affect absolute plaque size and vessel occlusion (percentage plaque area of total vessel area). B, vertical) Absolute and percentage collagen content of the plaque was determined by Masson's Trichrome staining. C, vertical) Absolute and percentage macrophage content of the plaque was determined by Monocyte/macrophage staining (clone MOMA-2). All representative pictures are taken at optical magnification 5x. Scale bars indicate 500 µm. Data are shown as mean ± SEM. * $p < 0.05$, ** $p < 0.01$, **** $p < 0.0001$.

Similar effects of BTK inhibition in a therapeutic study set-up

Since cardiovascular patients often already have established plaques and mast cells were previously seen to accumulate in the vessel wall during plaque progression[6,26], we also investigated the effects of BTK inhibition by Acalabrutinib in advanced-stage atherosclerosis by performing a therapeutic study. In this study, *Ldlr*$^{-/-}$ mice were first fed a high-fat diet for eight weeks to create existing plaques, before another eight weeks of high-fat diet and treatment with Acalabrutinib or control solvent (Supplement Figure 5). During this study, body weight and total serum cholesterol levels did not differ between the control and treatment group. In line with the prevention study, we observed a significant shift from FO I B cells towards FO II B cells in blood, spleen and mLNs of Acalabrutinib treated mice (Spleen FO II B cells: Acalabrutinib 90.2 ± 0.4%, control 87.9 ± 0.4% ($p = 0.002$); Spleen FO I B cells: Acalabrutinib 8.5 ± 0.5%, control 10.5 ± 0.5% ($p = 0.001$); Figure 4C), while total CD19^{+} B220^{+} B cell frequencies and B2 cell subsets remained largely unaffected (Figure 4A-B and Supplement Figure 6A-B). In this advanced atherosclerosis study, we did observe a significant decrease in circulating IgG2b levels and a trend towards a decrease in IgG1 levels (Supplement Figure 6C). Furthermore, we observed slightly higher peritoneal mast cell levels in Acalabrutinib treated mice compared to control mice. Peritoneal mast cell activation status however did not differ between the groups (Figure 4D). Additionally, adventitial mast cell numbers and activation status were also not affected in the aortic arch (Figure 4E) and aortic root (Figure 4F). Circulating monocytes and myeloid cells in the spleen also remained unaffected (Supplement Figure 7). As shown in Figure 5, Acalabrutinib treatment did not significantly affect atherosclerotic plaque size, collagen content (Supplement Figure 8) and monocyte/macrophage content when compared to control mice in a therapeutic study set-up.

Discussion

Atherosclerosis is the main pathology underlying CVD and there is an urgent need to discover new pharmacological treatments to prevent atherosclerotic plaque development and progression towards unstable plaques. In this study, we investigated BTK as a potential therapeutic target to limit mast cell activation and B cell maturation in atherosclerosis. Our single-cell RNA sequencing datasets of advanced human carotid artery plaques and mouse atherosclerotic aortic plaques show that, in line with literature, *BTK* is expressed in intraplaque mast cells, B cells and myeloid cells[21,22]. Therefore, we also assessed BTK as a therapeutic target in a mouse model for atherosclerosis. Here, we show that BTK inhibition in early and advanced atherosclerosis does not affect plaque size and composition, despite affecting follicular B cell maturation.

As mentioned before, BTK is well known for its crucial role in B cell development and B-cell receptor (BCR) signaling. Our data showed that BTK inhibition in early- and advanced-stage

atherosclerosis mainly affects the maturation of atherogenic follicular B cell subsets, without affecting systemic B cell frequencies and other B cell subsets. More specifically, we observed a shift from mature/activated FO I B cells towards less mature FO II B cells, which is in line with a study in which BTK was inhibited in a mouse model of MS[24]. Moreover, it is known that FO I B cell formation is a BCR driven and BTK-dependent process, which explains the effect on follicular B cell maturation upon BTK inhibition[27]. The biological effect on follicular B cell maturation in our atherosclerosis studies suggests that BTK was successfully inhibited. In addition, our data showed that Acalabrutinib treatment did not affect circulating antibody levels in the early atherosclerosis experiment, while reducing IgG levels in the advanced atherosclerosis study, where mice received a high-fat diet for a prolonged time. The role of IgG antibodies in atherosclerosis remains controversial, but is often described to be atherogenic[28], suggesting an atheroprotective effect of Acalabrutinib treatment in the therapeutic study. However, this effect on circulating antibodies did not translate in an effect on atherosclerotic plaque.

In atherosclerosis, follicular B cells are described to exert atherogenic functions, such as pro-inflammatory cytokine production, IgG antibody secretion and regulating T-cell responses, thereby contributing to plaque progression[13,28]. Previously, B cell targeting therapies have been investigated in the context of atherosclerosis[29,30]. For instance, depletion of all B cells in high-fat diet fed *ApoE*$^{-/-}$ and *Ldlr*$^{-/-}$ mice using an anti-CD20 monoclonal antibody reduced the development of atherosclerosis in the aortic root, suggesting an atherogenic role for B cells in atherosclerosis[31]. However, only targeting atherogenic B cell subsets, such as follicular B cells, would be a more advantageous approach in treating atherosclerosis compared to complete B cell depletion.

Next to the effects of BTK inhibition on B cells, we showed the potency of Acalabrutinib in inhibiting IgE-mediated mast cell activation *in vitro*. We observed a dose-dependent reduction in activated CD63^{+} mast cells upon BTK inhibition, which is in line with studies described by Dispenza and colleagues, who showed that Acalabrutinib reduced β-hexosaminidase release as measure for mast cell degranulation from human skin-derived mast cells[12]. Despite these encouraging effects on mast cell activation *in vitro*, Acalabrutinib treatment did not inhibit mast cell activation *in vivo*. Despite the treatment, we still observed the majority of mast cells being activated in the aortic root. This may be caused by activation via other mast cell activation pathways, for example via toll-like receptors, neuropeptides or complement components[9]. Human intraplaque mast cells may indeed also undergo non-IgE-dependent activation, since at least a fraction of these intraplaque mast cells was seen to be activated without IgE bound to the cell surface[9]. Alternatively, Acalabrutinib may not be able to sufficiently inhibit IgE mediated mast cell activation in the local plaque microenvironment, because it may not reach the plaque and adventitia in sufficient levels, although this dosage has been previously described for *in vivo* use[32]. Acalabrutinib has a relatively short half-life of

about 1.5 hours, however, it is able to exert prolonged inhibitory effects due to its covalent binding properties. A preclinical pharmacodynamic model of Acalabrutinib in mice showed that BTK was fully occupied in splenocytes three hours after a single dose, and after 24 hours, BTK occupancy was still around 50%, showing its prolonged efficacy *in vivo*[32].

Overall, Acalabrutinib treatment in *Ldlr*$^{-/-}$ mice did neither affect atherosclerotic plaque size nor composition. The effects of Acalabrutinib in early and advanced atherosclerosis could possibly be attributed to the differences in pathogenic mechanisms and (immune) cell types involved in atherosclerosis compared to other autoimmune diseases and B cell malignancies where Acalabrutinib was shown to be effective[17,24,33]. In CLL patients, dual-treatments combining a BTK inhibitor with a phosphatidylinositol 3-kinase δ inhibitor showed promising results[34]. In future research, combination therapies with other specific therapeutic targets, such as Lyn or Syk, may therefore be explored in the context of atherosclerosis as well.

Collectively, we showed that BTK inhibition alone did not affect mast cell activation in early and advanced stage atherosclerosis, despite the systemic biological effect on follicular B cell maturation.

Funding
I.B. is an Established Investigator of the Dutch Heart Foundation (2019T067). This work was also supported by the Dutch Heart Foundation grant number 2018T051 to A.C.F.

Declaration of competing interest
The authors declare no competing interests.

Author contributions
Esmeralda Hemme: conceptualization, executing animal experiments, data acquisition, data analysis and interpretation, writing - original draft. **Danique Biskop**: data acquisition, data analysis and interpretation, writing – review and editing. **Marie A.C. Depuydt**: data acquisition, writing – review and editing. **Virginia Smit**: data acquisition and data analysis. **Lucie Delfos**: data acquisition, writing – review and editing. **Mireia N.A. Bernabe Kleijn**: executing animal experiments. **Amanda. C. Foks**: supervision and funding acquisition. **Johan Kuiper**: supervision. **Ilze Bot**: conceptualization, data analysis and interpretation, writing - original draft, supervision, funding acquisition.

Data availability
The data presented in this article are available on request from the corresponding author. The human single cell RNA sequencing data presented in this article are retrieved from Depuydt et al. Circ Res. 2020[20].

References

1. Banach, M. *et al.* Impact of statin therapy on coronary plaque composition: a systematic review and meta-analysis of virtual histology intravascular ultrasound studies. *BMC Med.* **13**, (2015).
2. Bot, I., Shi, G. P. & Kovanen, P. T. Mast cells as effectors in atherosclerosis. *Arterioscler. Thromb. Vasc. Biol.* **35**, 265–271 (2015).
3. Krishnaswamy, G., Ajitawi, O. & Chi, D. S. The human mast cell: an overview. *Methods Mol. Biol.* **315**, 13–34 (2006).
4. Heikkilä, H. M. *et al.* Mast cells promote atherosclerosis by inducing both an atherogenic lipid profile and vascular inflammation. *J. Cell. Biochem.* **109**, 615–623 (2010).
5. Bot, I. *et al.* Perivascular mast cells promote atherogenesis and induce plaque destabilization in apolipoprotein E-deficient mice. *Circulation* **115**, 2516–2525 (2007).
6. Willems, S. *et al.* Mast cells in human carotid atherosclerotic plaques are associated with intraplaque microvessel density and the occurrence of future cardiovascular events. *Eur. Heart J.* **34**, 3699–3706 (2013).
7. Galli, S. J. & Tsai, M. IgE and mast cells in allergic disease. *Nat. Med.* **18**, 693–704 (2012).
8. Wezel, A. *et al.* Mast cells mediate neutrophil recruitment during atherosclerotic plaque progression. *Atherosclerosis* **241**, 289–296 (2015).
9. Kritikou, E. *et al.* Flow Cytometry-Based Characterization of Mast Cells in Human Atherosclerosis. *Cells* **8**, (2019).
10. Tsiantoulas, D. *et al.* Increased Plasma IgE Accelerate Atherosclerosis in Secreted IgM Deficiency. *Circ. Res.* **120**, 78–84 (2017).
11. Gilfillan, A. M. & Rivera, J. The tyrosine kinase network regulating mast cell activation. *Immunol. Rev.* **228**, 149–169 (2009).
12. Dispenza, M. C. *et al.* Bruton's tyrosine kinase inhibition effectively protects against human IgE-mediated anaphylaxis. *J. Clin. Invest.* **130**, 4759–4770 (2020).
13. Douna, H. & Kuiper, J. Novel B-cell subsets in atherosclerosis. *Curr. Opin. Lipidol.* **27**, 493–498 (2016).
14. Byrd, J. C. *et al.* Targeting BTK with ibrutinib in relapsed chronic lymphocytic leukemia. *N. Engl. J. Med.* **369**, 32–42 (2013).
15. Wang, M. L. *et al.* Targeting BTK with ibrutinib in relapsed or refractory mantle-cell lymphoma. *N. Engl. J. Med.* **369**, 507–516 (2013).
16. Honigberg, L. A. *et al.* The Bruton tyrosine kinase inhibitor PCI-32765 blocks B-cell activation and is efficacious in models of autoimmune disease and B-cell malignancy. *Proc. Natl. Acad. Sci. U. S. A.* **107**, 13075–13080 (2010).
17. Chang, B. Y. *et al.* The Bruton tyrosine kinase inhibitor PCI-32765 ameliorates autoimmune arthritis by inhibition of multiple effector cells. *Arthritis Res. Ther.* **13**, (2011).
18. Depuydt, M. A. C. *et al.* Single-cell T cell receptor sequencing of paired human atherosclerotic plaques and blood reveals autoimmune-like features of expanded effector T cells. *Nat. Cardiovasc. Res. 2023* 1–14 (2023) doi:10.1038/s44161-022-00208-4.
19. Hellings, W. E. *et al.* Histological characterization of restenotic carotid plaques in relation to recurrence interval and clinical presentation: a cohort study. *Stroke* **39**, 1029–1032 (2008).
20. Depuydt, M. A. C. *et al.* Microanatomy of the Human Atherosclerotic Plaque by Single-Cell Transcriptomics. *Circ. Res.* **127**, 1437–1455 (2020).
21. Zhu, S. *et al.* Multifaceted Immunomodulatory Effects of the BTK Inhibitors Ibrutinib and Acalabrutinib on Different Immune Cell Subsets - Beyond B Lymphocytes. *Front. cell Dev. Biol.* **9**, (2021).
22. Genevier, H. C. *et al.* Expression of Bruton's tyrosine kinase protein within the B cell lineage. *Eur. J. Immunol.* **24**, 3100–3105 (1994).
23. Kraft, S. *et al.* The tetraspanin CD63 is required for efficient IgE-mediated mast cell degranulation and

anaphylaxis. *J. Immunol.* **191**, 2871–2878 (2013).

24. Torke, S. *et al.* Inhibition of Bruton's tyrosine kinase interferes with pathogenic B-cell development in inflammatory CNS demyelinating disease. *Acta Neuropathol.* **140**, 535–548 (2020).
25. Weber, A. N. R. *et al.* Bruton's Tyrosine Kinase: An Emerging Key Player in Innate Immunity. *Front. Immunol.* **8**, (2017).
26. Laine, P., Naukkarinen, A., Heikkilä, L., Penttilä, A. & Kovanen, P. T. Adventitial mast cells connect with sensory nerve fibers in atherosclerotic coronary arteries. *Circulation* **101**, 1665–1669 (2000).
27. Cariappa, A. *et al.* The recirculating B cell pool contains two functionally distinct, long-lived, posttransitional, follicular B cell populations. *J. Immunol.* **179**, 2270–2281 (2007).
28. Smeets, D., Gisterå, A., Malin, S. G. & Tsiantoulas, D. The Spectrum of B Cell Functions in Atherosclerotic Cardiovascular Disease. *Front. Cardiovasc. Med.* **9**, (2022).
29. Kyaw, T. *et al.* Depletion of B2 but not B1a B cells in BAFF receptor-deficient ApoE mice attenuates atherosclerosis by potently ameliorating arterial inflammation. *PLoS One* **7**, (2012).
30. Kyaw, T. *et al.* Conventional B2 B cell depletion ameliorates whereas its adoptive transfer aggravates atherosclerosis. *J. Immunol.* **185**, 4410–4419 (2010).
31. Ait-Oufella, H. *et al.* B cell depletion reduces the development of atherosclerosis in mice. *J. Exp. Med.* **207**, 1579–1587 (2010).
32. Barf, T. *et al.* Acalabrutinib (ACP-196): A Covalent Bruton Tyrosine Kinase Inhibitor with a Differentiated Selectivity and In Vivo Potency Profile. *J. Pharmacol. Exp. Ther.* **363**, 240–252 (2017).
33. Neys, S. F. H., Hendriks, R. W. & Corneth, O. B. J. Targeting Bruton's Tyrosine Kinase in Inflammatory and Autoimmune Pathologies. *Front. cell Dev. Biol.* **9**, (2021).
34. De Rooij, M. F. M. *et al.* Ibrutinib and idelalisib synergistically target BCR-controlled adhesion in MCL and CLL: a rationale for combination therapy. *Blood* **125**, 2306–2309 (2015).

Supplementary data

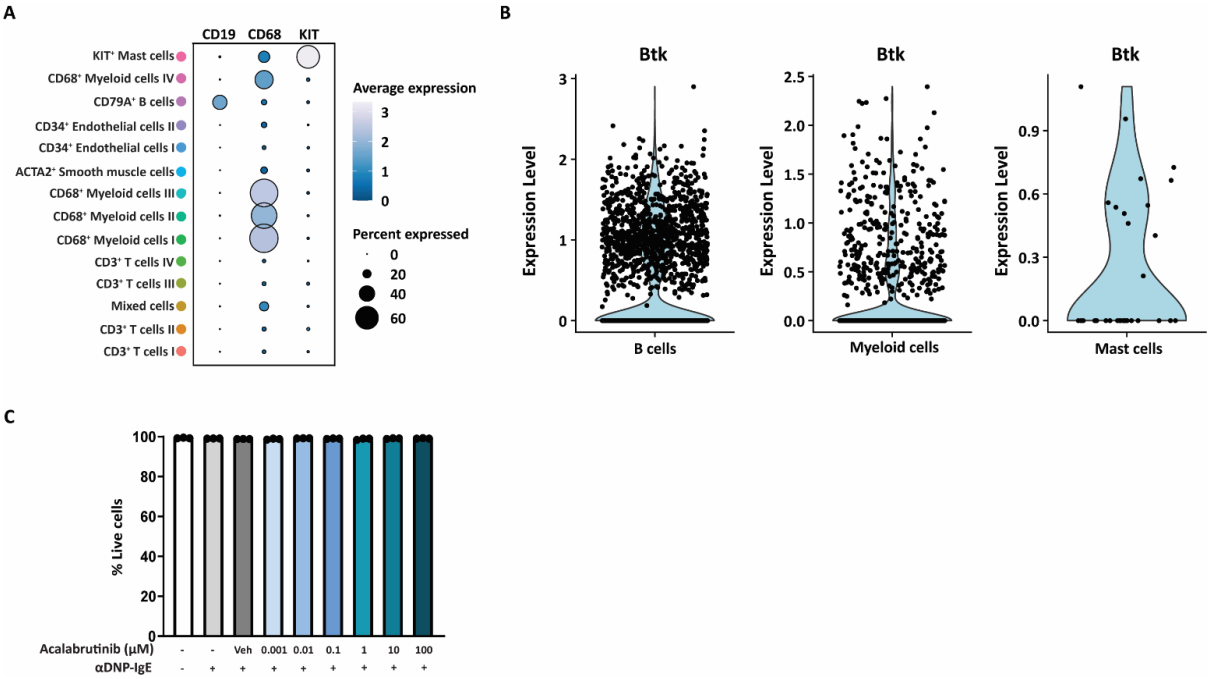

Supplement Figure 1. A) DotPlot visualization of signature genes *CD19*, *CD68* and *KIT* confirmed B cell (*CD19*), myeloid (*CD68*) and mast cell (*KIT*) cluster identities in human carotid artery plaques. B) Violin plot visualization of *Btk* expression in (*Cd19*$^{+}$) B cells, (*Cd68*$^{+}$ *Itgam*$^{+}$) myeloid cells and (*Kit*$^{+}$ *Cpa3*$^{+}$) mast cells in female *Ldlr*$^{-/-}$ atherosclerotic plaques. C) Acalabrutinib treatment did not induce bone marrow derived mast cell death as measured by a Live/Dead Fixable Viability marker using flow cytometry as viability remained at on average 98%. Data are shown as mean ± SEM.

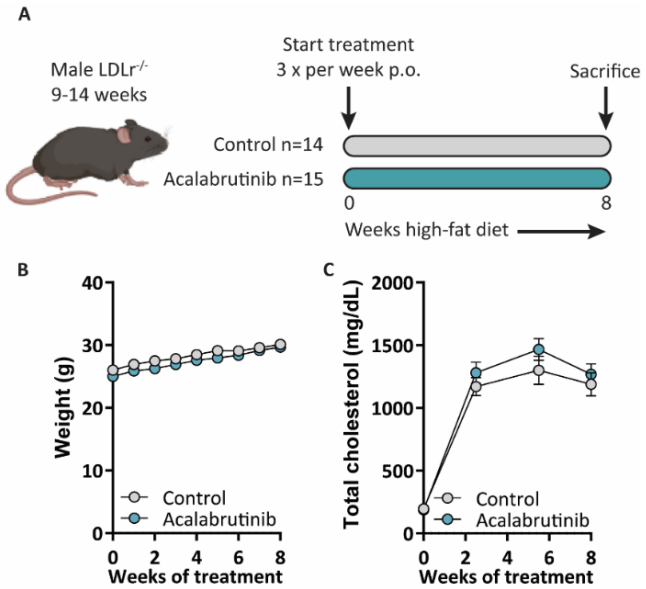

Supplement Figure 2. Acalabrutinib treatment did not affect body weight and serum total cholesterol levels in an atherosclerosis prevention study. A) Graphical overview of the prevention study set-up. Male *Ldlr*$^{-/-}$ mice were treated with Acalabrutinib (25 mg/kg; n=15) or control solvent (n=14) while being fed a high-fat diet (HFD). During the study, B) weight and C) serum total cholesterol levels were not affected by Acalabrutinib treatment. Data are shown as mean ± SEM.

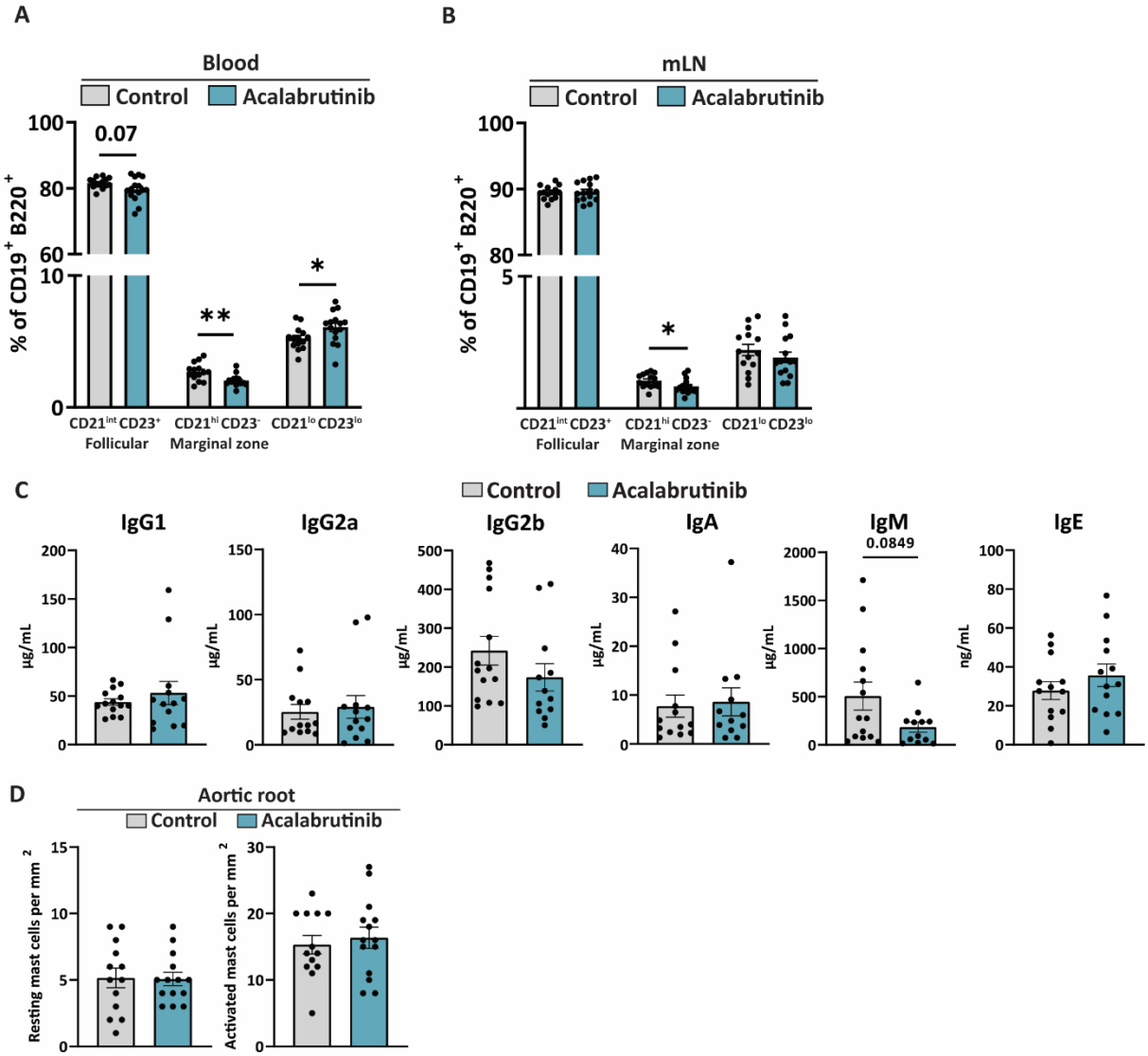

Supplement Figure 3. Acalabrutinib treatment decreased B cell maturation, but did not affect mast cell activation in a prevention *in vivo* set-up. Quantification of follicular ($CD21^{int}$ $CD23^{+}$), marginal zone ($CD21^{hi}$ $CD23^{-}$) and newly formed ($CD21^{lo}$ $CD23^{lo}$) B cells in A) the circulation and B) mLNs. C) Serum immunoglobulin (Ig) concentrations were measured. D) Histological quantification of resting (left) and activated (right) adventitial mast cells in the aortic root. Data represent mean ± SEM. * $p < 0.05$

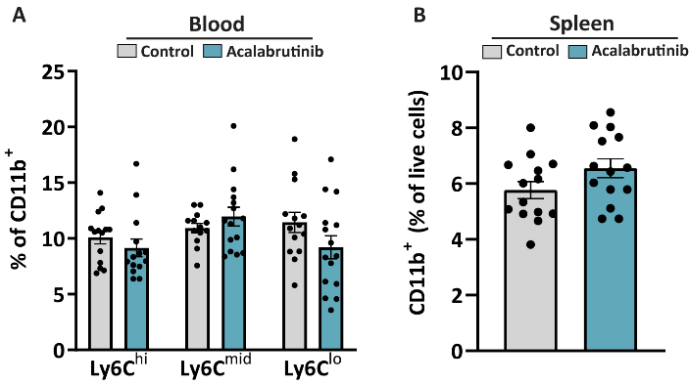

Supplemental Figure 4. Acalabrutinib treatment did not affect circulating monocytes and myeloid cells in the spleen in an atherosclerosis prevention study. A) Flow cytometry quantification of Ly6C^{hi}, Ly6C^{mid} and Ly6C^{lo} monocytes in the circulation. B) Flow cytometry quantification of myeloid cells (CD11b^{+}) in the spleen. Data represent mean ± SEM.

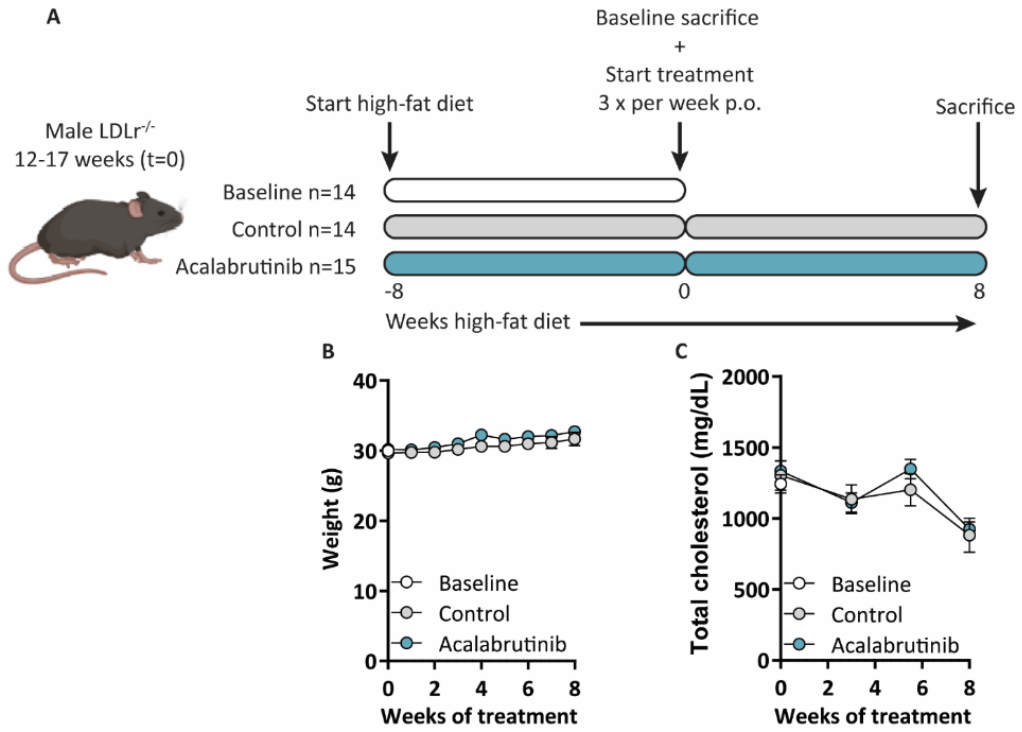

Supplement Figure 5. Acalabrutinib treatment did not affect body weight and serum total cholesterol levels in an atherosclerosis therapeutic study. A) Graphical overview of the therapeutic study set-up. Male *Ldlr*$^{-/-}$ mice were fed a high-fat diet (HFD) for eight weeks after which one group was sacrificed (baseline; n=14), while other mice were fed a HFD for another eight weeks while being treated with Acalabrutinib (25 mg/kg; n=15) or control solvent (n=14) for eight weeks. During the study, B) weight and C) serum total cholesterol levels were not affected by Acalabrutinib treatment. Data are shown as mean ± SEM.

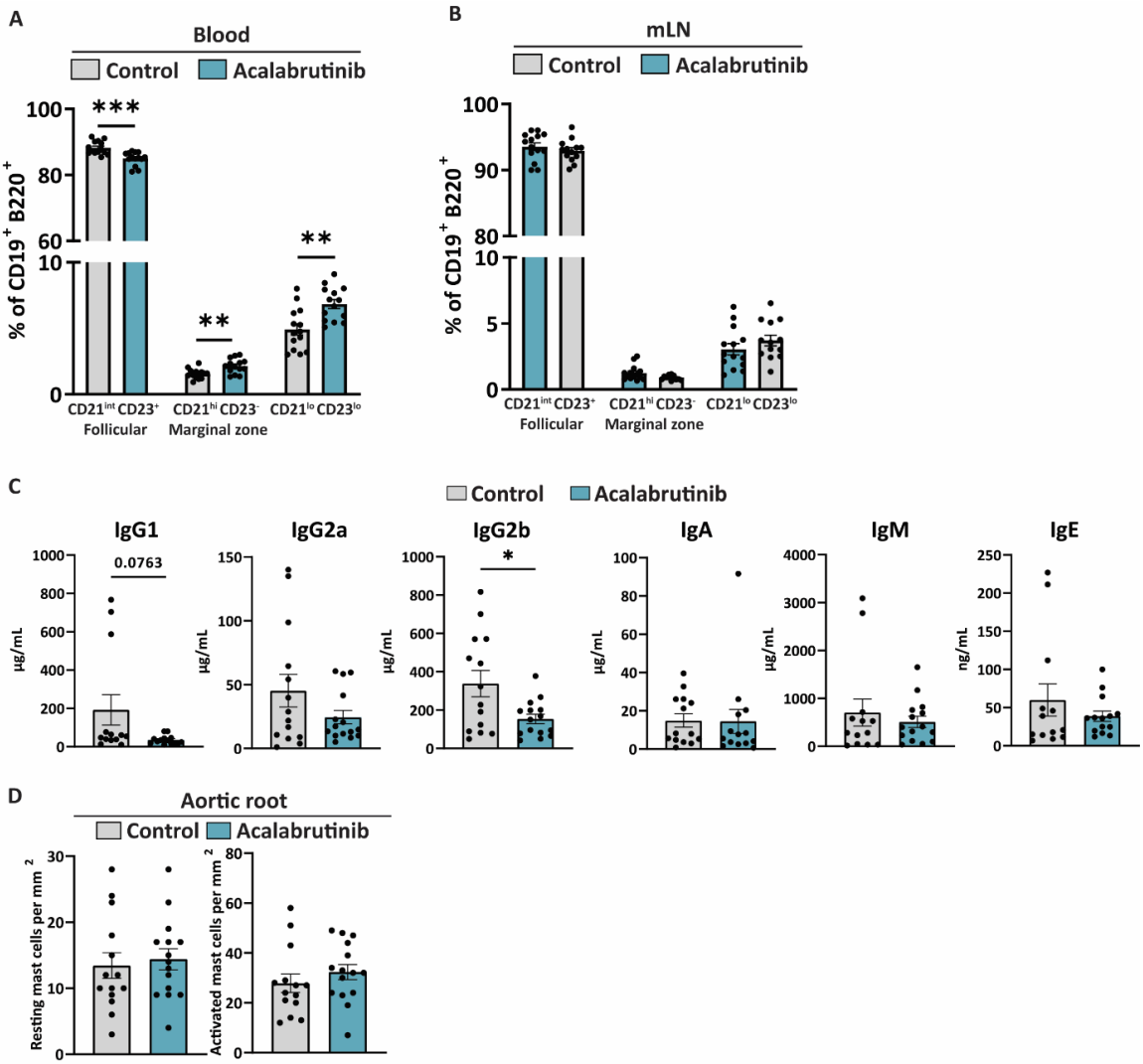

Supplement Figure 6. Acalabrutinib treatment decreased B cell maturation, but did not affect mast cell activation in a therapeutic *in vivo* set-up. Follicular ($CD21^{int}$ $CD23^{+}$), marginal zone ($CD21^{hi}$ $CD23^{-}$) and newly formed ($CD21^{lo}$ $CD23^{lo}$) B cells were quantified in in A) the circulation and B) mLNs, which revealed decreased frequency of follicular B cells in the circulation. C) Serum immunoglobulin (Ig) concentrations were measured. D) Histological quantification of resting (left) and activated (right) adventitial mast cells in the aortic root. Data represent mean ± SEM. * $p < 0.05$

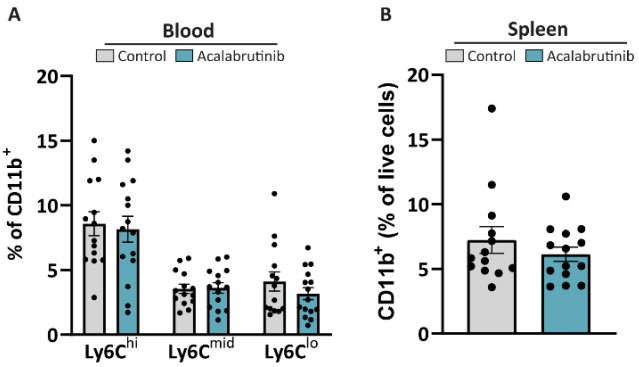

Supplemental Figure 7. Acalabrutinib treatment did not affect circulating monocytes and myeloid cells in the spleen in a therapeutic atherosclerosis study. A) Flow cytometry quantification of Ly6C^{hi}, Ly6C^{mid} and Ly6C^{lo} monocytes in the circulation. B) Flow cytometry quantification of myeloid cells (CD11b^{+}) in the spleen. Data represent mean ± SEM.

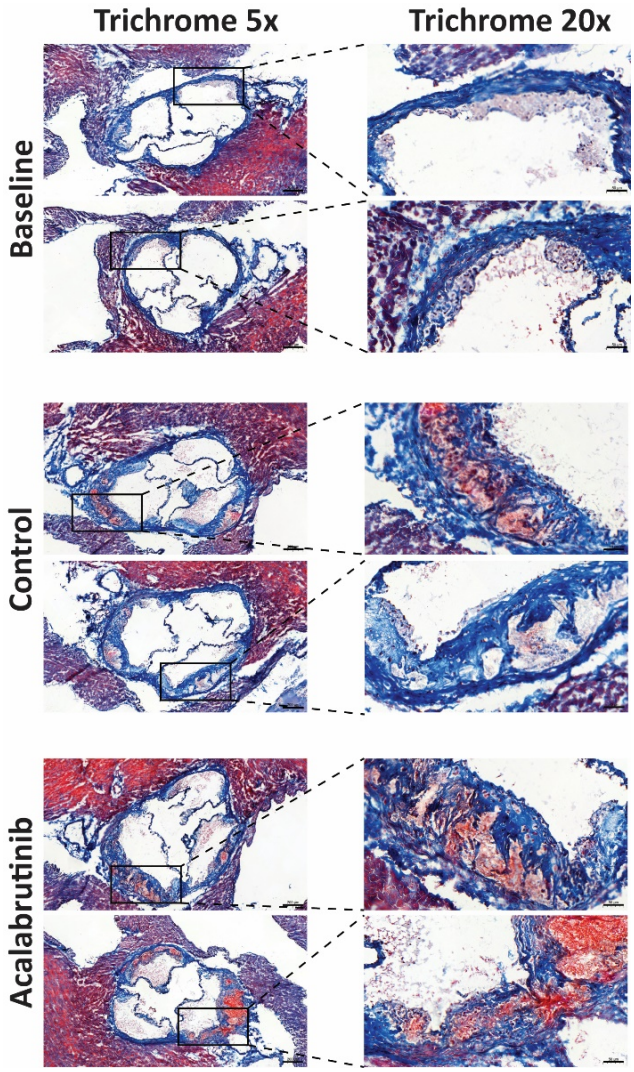

Supplement Figure 8. Masson's Trichrome staining to determine collagen content of the plaque in the therapeutic study. Representative pictures of the three-valve area of the aortic root are taken at optical magnification 5x (left pictures). Representative pictures of enlarged areas are taken at optical magnification 20x (right pictures). Black boxes indicate enlarged areas. Scale bars (left) indicate 200 µm. Scale bars (right) indicate 50 µm.

Table S1. Flow cytometry antibodies

Marker	Fluorochrome	Clone	Supplier
CD21	BV421	7E9	Biolegend
B220	BV510	RA3-6B2	Biolegend
CD19	BV605	6D5	Biolegend
CD27	BV650	LG.3A10	Biolegend
IgM	FITC	II/41	eBioscience
CD93	PerCP-Cy5.5	AA4.1	Biolegend
CD23	PE	B3B4	Biolegend
IgD	APC	11-26c.2a	Biolegend
CD45	AF700	30-F11	Biolegend
CD45	eFluor450	30-F11	eBioscience
CD19	PerCPCy5.5	eBio1D3	eBioscience
Thy1.2	PerCPCy5.5	53-2.1	Biolegend
CD117	PE	2B8	Biolegend
CD63	APC	NVG-2	eBioscience
FceRI	AF700	MAR-1	Biolegend
CD11b (Figure S4)	PE	M1/70	Biolegend
Ly6C (Figure S4)	PE-CF594	AL-21	BD Biosciences
CD11b (Figure S6)	BV605	M1/70	Biolegend
Ly6C (Figure S6)	APC	HK1.4	eBioscience
Fixable Viability Dye	AF780		Biolegend
CD16/CD32		93	Biolegend

Table S2. Flow cytometry markers used for leukocyte identification.

Cell type	Flow cytometry markers
Mast cells	$CD45^+$ Lineage (CD19, Thy1.2)$^-$ $CD117^+$ $Fc\varepsilon RI^+$
Activated mast cells	$CD45^+$ Lineage (CD19, Thy1.2)$^-$ $CD117^+$ $Fc\varepsilon RI^+$ $CD63^+$
B cells	$CD19^+$ $B220^+$
Follicular B cells	$CD19^+$ $B220^+$ $CD93^-$ $CD21^{int}$ $CD23^+$
Marginal zone B cells	$CD19^+$ $B220^+$ $CD93^-$ $CD21^{hi}$ $CD23^-$
Newly formed B cells	$CD19^+$ $B220^+$ $CD93^-$ $CD21^{lo}$ $CD23^{lo}$
Immature follicular II B cells (FOII)	$CD19^+$ $B220^+$ $CD93^-$ $CD21^{int}$ $CD23^+$ IgM^{hi} IgD^{hi}
Mature follicular I B cells (FO I)	$CD19^+$ $B220^+$ $CD93^-$ $CD21^{int}$ $CD23^+$ IgM^{lo} IgD^{hi}
Inflammatory monocytes (high)	$CD11b^+$ $Ly6C^{hi}$
Inflammatory monocytes (middle)	$CD11b^+$ $Ly6C^{mid}$
Patrolling monocytes	$CD11b^+$ $Ly6C^{lo}$
Myeloid cells	$CD11b^+$